

TAYLOR VORTICES FLOW IN PARTIALLY-OBSTRUCTED ANNULAR SPACE WITH INNER CYLINDER ROTATION

Bruno Venturini Loureiro

Department of Mechanical Engineering, PUC-RIO
22453-900, Rio de Janeiro, Brazil
brunovl@ucl.br

Paulo Roberto S. Mendes

Department of Mechanical Engineering, PUC-RIO
22453-900, Rio de Janeiro, Brazil
pmendes@mec.puc-rio.br

Luis Fernando A. Azevedo

Department of Mechanical Engineering, PUC-RIO
22453-900, Rio de Janeiro, Brazil
lffa@mec.puc-rio.br

Abstract. *The present work studies the characteristics of the flow field inside an annular space formed by two concentric cylinders with rotation of the inner cylinder. The annular space was partially blocked by a plate parallel to the axis of rotation, thereby destroying the circumferential symmetry of the annular space geometry. This flow configuration encounters application in the modeling of drilling of horizontal petroleum wells where a bed of cuttings is formed at the bottom part of the annulus. This bed was modeled in the present work by a flat plate inserted into the annular space. The velocity field was investigated both numerically and experimentally. The equations governing the three-dimensional, laminar flow of a Newtonian fluid were solved via a finite-volume technique. The instantaneous and time-averaged flow fields over two-dimensional meridional sections of the annular space were measured employing the particle image velocimetry technique (PIV). Attention was focused on the determination of the onset of secondary flow in the form of distorted Taylor vortices. The results demonstrated that the critical rotational Reynolds number is directly influenced by the degree of obstruction of the flow given by the cylinder-to-plate gap. The smaller the gap, the larger the critical rotational Reynolds number. The gap dimensions control the width of the vortices. Transition values of the rotational Reynolds numbers were well predicted by the computations. Differences were found between measured and predicted values for the length of the Taylor vortices. Transverse flow maps revealed a complex interaction between Taylor vortices and zones of recirculating flow, for moderate to high degrees of flow obstruction.*

Keywords. Taylor vortex, partially-obstructed annular space, particle image velocimetry.

1. Introduction

The flow field generated in the annular region formed by two concentric cylinders due to the rotation of the inner cylinder is a classical problem in fluid mechanics that has received considerable attention in the literature. The flow instabilities generated in the annular space have been investigated since the pioneer work of Taylor (1923). Since then, several other works addressed different features of this super critical Couette flow, Cole (1976) and DiPrima (1984). Andereck et al. (1986) characterized the super critical flow regimes in circular Couette flow, while Wereley and Lueptow (1998) employed whole field techniques to measure the flow field in a meridional plane.

Besides its fundamental importance, super critical circular Couette flow encounters several important practical applications. The present research was motivated by an application of circular Couette flow to the drilling of horizontal oil and gas wells. Horizontal wells have been extensively used in recent years by the petroleum industry due to higher efficiency in oil recovery from the reservoirs that can be obtained with this technology, when compared to the classical vertical well technology. A challenge posed to the horizontal drilling technique is the ability of efficiently remove the solid materials resultant from the drilling operation that tend to settle and accumulate at the lower part of the annular space formed by the well wall and the rotating drilling shaft. The design of a successful operation relies on simulations of the capability of the flow of drilling fluids of suspending and removing the bed of cuttings formed. One of the key inputs to such simulations are the velocity profiles that prevail in the annular space. Most of the times, due to the complexity of an actual operation, crude approximations for the velocity profile – such as plug flow – are employed. There are a few works in the petroleum literature that deal with the influence of shaft rotation on the flow field and horizontal well cleaning efficiency, Lockett et al. (1993), Philip et al. (1997), and Sifferman et al. (1992).

The present paper reports on the efforts of an ongoing project aimed at studying the flow field and cleaning characteristics of horizontal wells. In the first phase presented here, a simplified model of the problem is studied in detail. The model considers an annular space formed by an outer fixed cylinder and an inner rotating cylinder of large length-to-gap ratio. The annular space is limited by end walls. No axial flow is present. The bed of cuttings is modeled by a horizontal wall that partially obstructs the annular gap, as can be seen schematically in Fig. 1.

In the flow in an annular space with rotation of the inner cylinder, the transition from laminar Couette flow to turbulent flow is characterized by four regimes, according to Andereck et al. (1986): i) Couette flow, ii) Taylor vortex

flow, iii) wavy-vortex flow and iv) modulated vortex flow. An additional regime was identified and reported in Lim et al (1998). This regime occurs between Taylor and wavy vortex flow, and was named secondary Taylor vortex flow. These five regimes are characterized by a rotational Reynolds number, a ratio of inner to outer annulus radius and, for some regimes, by the acceleration imposed on the inner cylinder to reach the steady state rotation level desired.

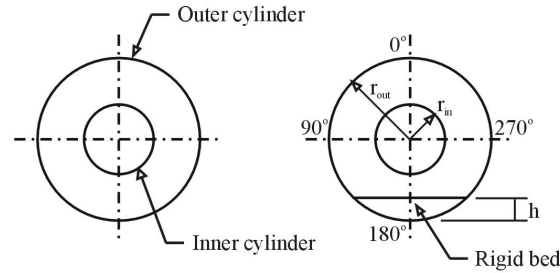


Figure 1. Transversal section of the partially-obstructed annular space geometry.

The effect of the annular space radius ratio on the Couette stability was investigated mathematically by DiPrima et al. (1998) for concentric, infinite length cylinders. DiPrima et al. have shown that the critical rotational Reynolds number that characterizes the onset of Taylor vortex flow increases with the radius ratio, for radius ratios larger than 0.45.

Park et al. (1981) and Anderec et. al. (1986) demonstrated that the transition from Couette to Taylor vortex flow depends on the acceleration ramp imposed on the inner cylinder. Park et al. obtained a hysteresis curve for the critical Reynolds number by approaching the transition point either increasing or decreasing the cylinder rotation. They have also reported that the hysteresis effect is negligible if the dimensionless acceleration imposed is smaller than 10. The dimensionless acceleration is defined by Park et al. (1981) as,

$$a^* = \frac{d Re}{dt^*} \cdot \frac{1}{\Gamma} \quad \text{with} \quad t^* = \frac{t}{(L^2/\nu)}, \quad \Gamma = L/d \quad (1)$$

Cole (1976) employed a visualization technique to study the influence of the annular space length-to-gap aspect ratio on the Taylor-vortex and wavy-vortex instabilities. He has found that the onset of Taylor-vortex instability is not affected for aspect ratios larger than 20, and larger than 50 for the wavy-vortex instabilities.

The effect of the eccentricity between the inner and outer cylinders on the Taylor vortex instability was investigated by DiPrima and Stuart (1972) and Eagles et al. (1978). Both works report that the value of the critical Reynolds number that characterizes the onset of Taylor-vortex instability increases with eccentricity.

The objective of the present work is to determine the influence of the partial obstruction of the annular gap on the flow structure within the gap. To this end, a combined experimental and numerical program was conducted where instantaneous, whole-field velocity measurements and three-dimensional computer simulations were employed to help characterize the flow field. A natural continuation of the present study would include the features of the problem that occur in the actual application such as, imposed axial flow, non Newtonian fluid and a non-rigid bed of cuttings.

2. Governin equations and numerical solution

The problem investigated is characterized by two horizontal, concentric cylinders forming an annular space with inner radius r_i and an outer radius r_o , defining the annular space of dimension $d = r_o - r_i$. The outer cylinder is fixed, while the inner cylinder rotates with an angular velocity Ω . A horizontal plate is placed at the lower part of the annular space, at a distance h from the external radius. The length of the annular space, L , is the same as that of the plate. A view of the cross section of the partially obstructed geometry studied is shown in Fig. 1. Although solutions for infinitely-long annular spaces were desired, the need to compare the numerical solutions with experiments required that the annular space was confined by two vertical end walls.

The governing equations for an incompressible, Newtonian fluid, with constant properties, flowing at steady state conditions, are given by the mass conservation and Navier-Stokes equations,

$$\vec{\nabla} \cdot \vec{u} = 0 \quad (2)$$

$$\vec{u} \cdot \vec{\nabla} \vec{u} = -\frac{1}{\rho} \vec{\nabla} p + \nu \vec{\nabla}^2 \vec{u} \quad (3)$$

In the above equations, \vec{u} , is the velocity vector, p , the fluid pressure, ρ and ν are, respectively the fluid density and kinematic viscosity.

The presence of the horizontal plate in the annular space destroys the circumferential symmetry of the classical circular Couette problem. Therefore, when the plate is present, a three-dimensional solution should be obtained. The dimensionless parameters that govern the problem are the rotational Reynolds number based on the inner cylinder angular velocity, $Re = \Omega r_i d / \nu$, the inner-to-outer cylinder radius ratio, $\eta = r_i / r_o$, the annular space length-to-gap aspect ratio, $\Gamma = L/d$, and the dimensionless obstruction h/d .

The boundary conditions employed in the solution of the problem were the no-slip conditions at the inner and outer cylinder walls. At the vertical walls that confine the annular space two types of boundary conditions were tested. The first kind of boundary condition tested was no-slip at the vertical walls. This condition models the experimental test section constructed. The second type of boundary condition was used as an attempt to simulate the fluid flow in infinitely long annular spaces. To this end, the boundary condition suggested by Coronado-Mattuti et al. (2004) was implemented. In this condition, the computational domain is extended and no-slip boundary conditions are imposed at the new solid surfaces. At the surface of the inner cylinder that belongs to the extended computational domain the angular velocity is set to zero. This approach provides essentially an additional cavity of fluid that allows freedom to accommodate the vortical flow in the annular space. Coronado-Mattuti et al. (2004) reported good results employing this type of boundary condition.

In order to optimize memory space and computer time, some numerical solutions were performed employing a symmetry boundary condition at the annular space mid-length. The results obtained with the three boundary conditions described were tested against the experimental results. In order to facilitate future reference in the paper, these boundary conditions were labeled as:

- Type (a) boundary condition: symmetry at mid-length and extended domain at vertical end plane;
- Type (b) boundary condition: symmetry at mid-length and no-slip condition at vertical end wall;
- Type (c) boundary condition: no-slip condition at both vertical end walls (Computation of the full domain).

The conservation equations together with the appropriate boundary condition were solved numerically employing the software Fluent version 6.12. This code employs a finite-volume-based discretization of the governing equations, using a power-law interpolation scheme. The pressure-velocity coupling utilized was the SIMPLE algorithm, according to Patankar (1980). The resulting algebraic system is solved using a multi-grid procedure. Extensive mesh sensitive tests were conducted in order to define an appropriate three-dimensional mesh for solving the problem. Grid independence was obtained for a uniform mesh of $25 \times 160 \times 400$ control volumes, deployed, respectively, in the radial, circumferential and axial directions.

3. Experimental setup

The experimental setup to be described next was designed and constructed with the objective of allowing the assessment of the influence of the cylinder-to-plate gap on the flow structure inside the annular region, and on the critical rotational Reynolds number that characterizes the transition to the vortex flow regime.

3.1. Test section

Figure 2 is a schematic representation of the test section employed in the experiments. Capital letters in the figure mark some components of the test section to facilitate the description in the text.

A horizontal aluminum hollow shaft (A) was mounted concentrically with a 5-mm-thick Plexiglas cylinder (B). The outer diameter of the shaft was 125 mm, while the inner diameter of the Plexiglas cylinder was equal to 220 mm, thereby forming an annular gap of 47.5 mm. The inner aluminum shaft was machined from a 5-mm-thick extruded pipe. One aluminum cap with a protruding 25-mm-diameter shaft was installed at each end of the hollow aluminum shaft. During the machining operation, the aluminum shaft was supported on the lathe by its two end-shafts, in order to guarantee a perfect rotation of the outer surface of the aluminum shaft around its centerline. At the end of the machining operation, a dial gauge was used to verify that the aluminum shaft rotated with an eccentricity smaller than 0.1 mm. The two end shafts were mounted on ball bearings (D) fixed on Plexiglas discs (C). Each disc was equipped with an O-ring and fixed to one of the end planes of the Plexiglas cylinder sealing the working fluid in the annular space. The length of the annular space formed was equal to 2475 mm, which produced a length-to-gap aspect ratio, L/d , of the order of 52. The ratio of the external inner cylinder diameter to the internal outer cylinder radius, r_i / r_o , was equal to 0.565.

An electrical motor equipped with a programmable speed control was used to rotate the aluminum shaft. Two pulleys connected with a synchronizing rubber belt were used to drive the aluminum shaft, providing a transmission ration of 7:1. The motor speed control and the low transmission ratio allowed for a smooth control of the shaft angular speed and speed rump up. As will be commented in the results section, the ability to control the shaft angular acceleration is critical for the success of the flow transition experiments performed. An encoder (E) was installed at the

tip of the aluminum shaft to monitor its angular motion. The encoder signal was registered by a computer that calculated angular displacement, angular velocity and acceleration of the shaft. As will be commented shortly, the signal from the encoder was also used to trigger the system used for measuring the instantaneous flow field.

A progressive cavity pump (F) was installed to aid in the preparation of the experiments. The pump was used to fill the annular cavity with the working fluid. In this operation, the working fluid was pumped from a reservoir (G) to the interior of the annular space, by opening valves (H), (I) and (J) and closing valves (L) and (K). Air was purged from the annular space using valve (M). The working fluid was formed by a mixture of glycerol, water and a few grams of small, silver coated, hollow glass spheres used as tracers for the laser technique employed. The pump was also used to circulate the working fluid prior to the data taken period in order to keep the tracer particles in suspension. The pump was not used during the experiments.

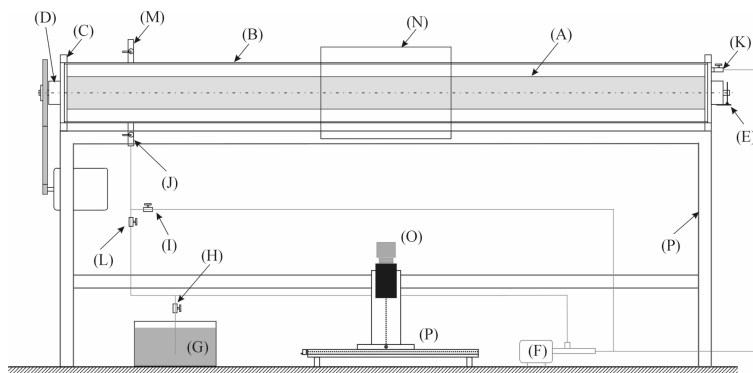


Figure 2. Schematic view of the experimental setup.

A Plexiglas box (N) was mounted around the Plexiglas tube with the objective of minimizing the distortions of the image in the annular space due to the curved wall. The box was filled with the working fluid, without the small hollow glass spheres, what provided a good matching to the index of refraction of Plexiglas. Two of the box walls were made of borosilicate glass. The laser sheet of the velocity measuring system entered through one of the vertical walls, while the images of the illuminated tracer particles were captured through the second, horizontal, lower glass wall.

The focus of the work was on the effect on the flow field within the annular gap caused by the presence of a partial obstruction placed within the gap. A set of five, 4-mm-thick Plexiglas plates was carefully machined to serve as the obstruction in the annular gap. The length of each plate matched the length of the annular gap. The width of each plate was calculated so as to produce the cylinder-to-plate spacing required for each particular experiment. The plate was introduced in the annular space by removing one of the Plexiglas end caps that sealed the annular space. The edges of the plates were beveled at an angle that matched the internal curvature of the Plexiglas cylinder, producing a smooth transition - without any appreciable step - from the curved internal wall of the cylinder to the horizontal top surface of the plate. The horizontal plates were fixed in position by a series of bolts that passed through the external surface of the Plexiglas cylinder and matched tapped holes in the inferior surface of the plate.

The complete assembly formed by the inner aluminum shaft, Plexiglas outer cylinder with horizontal plate (when present) and visualization box was mounted on a solid steel frame that was fixed to the laboratory floor using four anti-vibration bases. The assembly was fixed on the steel frame by mounting the Plexiglas cylinder on four semi-circular Plexiglas bases. Braces fixed the Plexiglas cylinder on the bases. When the braces were not yet tightened, it was possible to rotate the Plexiglas cylinder by hand. The rotation of the cylinder was only necessary in the experiments that used the horizontal plate in the annular gap. In these experiments, the circumferential symmetry of the flow in the annular space is destroyed and there is a need to measure flow fields in the r - z plane for different circumferential positions θ . This was achieved in the experiments conducted by keeping the illuminating laser sheet horizontal and positioning the Plexiglas cylinder at different circumferential coordinates. It should be mentioned that the visualization box was designed so that the Plexiglas cylinder could be circumferentially moved, while keeping the box in a fixed position with its vertical glass windows orthogonal to the incident laser sheet.

3.2. Velocity measurements

Time-resolved and average flow fields in the annular gap were obtained employing the Particle Image Velocimetry technique, PIV (e.g., Raffel et al., 1998). In this technique, a pulsed laser sheet illuminates small tracer particles previously distributed in the fluid. A digital camera, mounted orthogonally to the laser sheet captures the particle positions at two consecutive time instants. An image-processing algorithm calculates the displacements of small groups of particles in the image what, together with the time interval of image capture, produces the desired instantaneous flow field.

In the present study the PIV system used was manufactured by TSI Inc. The system employed a New Wave Research, 120 mJ per pulse, double-cavity laser that is able to fire double pulses at 15 Hz. The minimum time interval between pulses can be adjusted to a few nanoseconds, much less than necessary for the present low-speed experiments. Lenses attached to the laser unit transformed the beam into a divergent laser sheet with an approximate thickness at the beam waist of 0.3 mm. The tracer particles used were silver-coated, hollow glass spheres with mean diameter of 13 μm and density of 1.6 g/cm^3 , even though the working fluid density was approximately equal to 1.2 g/cm^3 , a very small number of particles was observed to settle over a 24-hour period. The camera (O) used to capture the particle images (TSI model PIVCAM 10-30) had 1000 x 1000 pixel resolution, working at 30 frames per second. This camera was mounted on a x-y-z coordinate table (P). Synchronization between laser firing and image capture was accomplished by a TSI model 60030 synchronizer. In the experiments conducted, instantaneous flow fields were captured as the aluminum shaft was accelerated from rest up to the final angular speed desired for a particular experiment. These measurements were accomplished by using the signal from the shaft encoder as a trigger for the TSI synchronizer.

Two types of velocity measurements were obtained: flow fields in the r-z plane and in the r- θ plane. In the former case, the light sheet was placed horizontally and the camera vertically. The tracer particles in this case crossed the light sheet with elevated circumferential velocity, especially in the regions close to the aluminum shaft surface where the velocity is highest. The time interval between laser pulses was adjusted so as to guarantee that the particles did not leave the light sheet during the two pulses, and still display a reasonable displacement to allow an accurate measurement. For the r- θ plane velocity measurements the laser sheet was set vertically and the camera horizontally. The images of the particles were captured through the Plexiglas end-caps of the Plexiglas cylinder. No experimental results for the r- θ plane velocity will be presented in the present paper.

A cross-correlation-based algorithm was employed to determine the particle displacement field. The algorithm was part of the software Insight version 5.0 developed by TSI Inc. Interrogation windows of 64x64 pixels displaced by 32 pixels were used in the calculations. An image calibration procedure indicated that the chosen interrogation window corresponded to a 3 x 3 mm window in the actual flow. Typically, 50 x 30 (axial x radial direction) velocity vectors were measured in each plane. The quality of the images obtained was such that the interrogation windows generated only valid vectors, so no vector interpolation scheme was employed. Average velocity fields were obtained by averaging over 100 measured vector fields. Calibrating experiments previously conducted with a solid body rotation apparatus indicated that the experimental accuracy for the PIV system employed is of the order of $\pm 1\%$, (Gomes et al., 2000).

4. Effects of angular acceleration on Taylor vortex onset

As already mentioned in the introduction, Park et al. (1981) demonstrated the effect of angular acceleration on the critical value of the rotational Reynolds number. A series of experiments was carried out to determine the relationship between angular acceleration and Taylor vortex onset for the annular region without the partial blockage. In these experiments the aluminum shaft was started from rest and slowly accelerated to reach a steady state condition. The shaft encoder recorded the rotation history and sent a signal to trigger the PIV system at every three shaft revolutions. The r-z velocity fields recorded were carefully examined to detect the onset of radial or axial velocities, which were the indication of the onset of Taylor vortices. Figure 3 presents the results obtained. In the figure, the critical rotational Reynolds number is plotted as a function of the dimensionless acceleration.

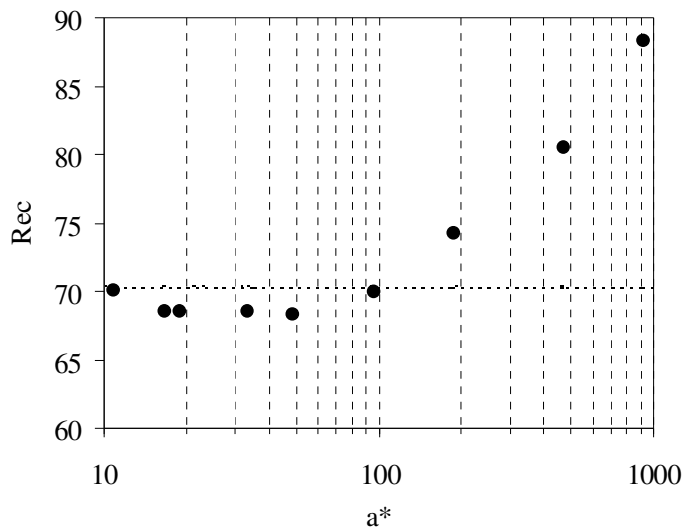


Figure 3. Influence of dimensionless acceleration on critical Reynolds number.

The influence of the acceleration on the value of the critical Reynolds number is clearly noted. For the lowest value of the acceleration tested, the value of the critical Reynolds number slightly over 70 agrees with data from the literature available for a radius ratio of $\eta = 0.55$, which is close to the value of the present study (DiPrima, 1984). All the experiments reported in the present paper were conducted with the minimum possible dimensionless acceleration value allowed by the experimental setup, which was around 10. This value is in accordance with the maximum limit suggested by Park et al. (1981) to minimize hysteresis effects on Taylor vortex transition values.

5. Taylor vortex onset for partially obstructed annular space

The onset of Taylor vortex flow in the partially obstructed annular space was investigated both numerically and experimentally. In the experimental tests, the same methodology described in the previous section was employed for determining the critical rotational Reynolds number values.

In the numerical investigations the three dimensional, steady state flow field was obtained for increasing values of the rotational Reynolds number until the onset of Taylor vortex flow was detected. The criteria employed for detecting the onset of Taylor vortex flow was that suggested by Coronado-Mattuti et al. (2004). According to this criterion, the ratio of the norm of the axial velocity field by the norm of the circumferential velocity field is calculated for each value of the rotational Reynolds number. Eq. (4) defines this ratio,

$$\frac{\|v_z\|}{\|v_\theta\|} = \frac{\sum_i^n |v_z|}{\sum_i^n |v_\theta|} \quad (4)$$

In the three dimensional calculations, the ratio defined by Eq. (4) was evaluated only over the node points contained in the meridional vertical planes (0 and 180°). For a flow configuration below the critical Reynolds number value, it is expected that the ratio of velocity norms be zero, indicating the presence only of the circumferential and radial velocity components. As the Taylor vortex structure begins to develop, axial components of the velocity will appear and the ratio of norms will increase.

Figure 4(a) presents the results obtained from the numerical simulations conducted. In the figure, the ratio of norms is plotted as a function of the rotational Reynolds number. The departure from zero can be detected for a Reynolds number around 75. A more accurate detection of the critical Reynolds number can be obtained if the derivative of the function is calculated and plotted in terms of the Reynolds number. This is presented in Fig. 4(b). The peak in the derivative of the norm function with respect to Reynolds clearly determines the transition point. This methodology was adopted in the present study.

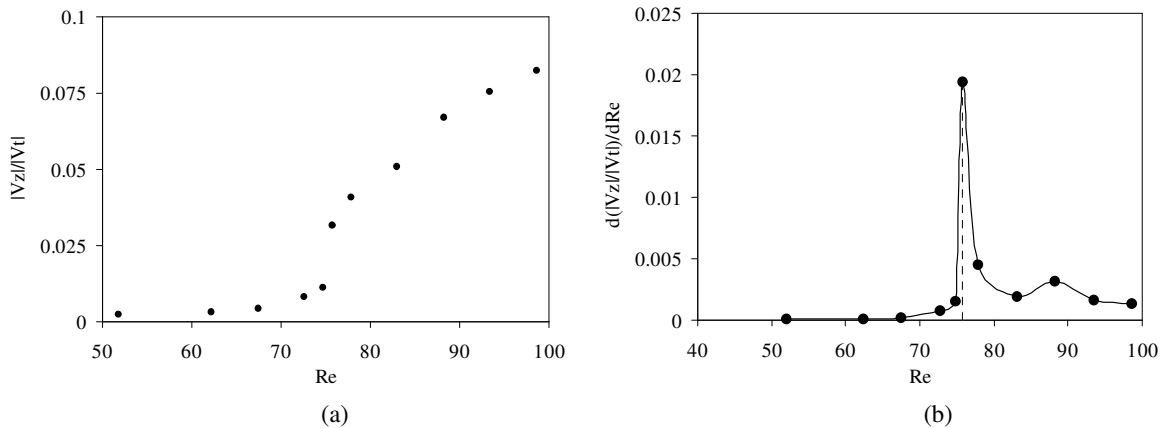


Figure 4. (a) Axial to tangential velocity ratio versus rotational Reynolds number; (b) Axial to tangential velocity ratio derivative versus rotational Reynolds number. $h/d = 0.25$

The effect of the flow obstruction on the critical Reynolds number will now be examined. Fig. 5 presents both the numerical and experimental results obtained for the critical rotational Reynolds number as a function of the dimensionless parameter, h/d , that characterizes the flow obstruction placed in the annular gap. One should recall that, according to Fig. 1, h is the distance from the outer surface of the annular space to the obstructing plate. According to this definition, a value of h/d equal to 1 corresponds to a complete obstruction of the annular space, while h/d equals to zero relates to the free annular space, i.e., without any obstruction.

An observation of Fig. 5 reveals that the obstruction of the annular space delays the transition to Taylor vortex flow regime. Indeed, the critical Reynolds number value for the free annular space of roughly 70 increases up to 145 for the maximum studied value of the obstruction given by $h/d = 0.75$. A plausible explanation for this behavior is that the obstruction of the flow requires a larger circumferential momentum in order to develop the radial components of the flow at a narrower annular gap passage.

Another observation to be made about the results of Fig. 5 is the remarkable agreement between experiments and computation. Indeed, the average deviation observed between experiments and computation is of the order of 0.9 %, the maximum deviation being 1.83 %. The average absolute experimental uncertainties estimated for the Reynolds number were of the order of 0.5.

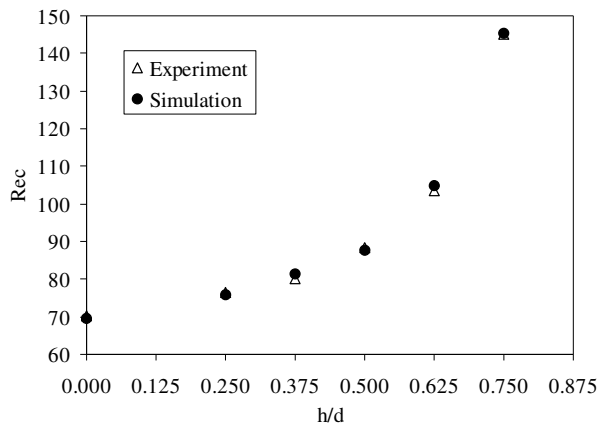


Figure 5. Critical Reynolds number versus annular obstruction for experimental and numerical simulation results.

The results of Fig. 5 allow the calculation of the ratio of the critical Reynolds number for the obstructed annular space, to the critical Reynolds number for the free annular space. This ratio is close to 1 up to $h/d = 0.3$ increasing abruptly to 2, for $h/d = 0.75$. These results can be of significant importance for the application that motivated the present work and mentioned in the introduction. Indeed, the rate of removal of particles forming a horizontal bed in an annular space can be directly influenced by the presence and intensity of Taylor vortices.

6. Taylor vortex characterization: vortex length

The determination of the influence of the obstruction in the annular space on the Taylor vortices length was investigated both numerically and experimentally. In both cases, the methodology employed to determine the vortex length was similar. The velocity field, determined either numerically or experimentally, was searched along a line of constant radial coordinate close to the inner rotating cylinder. The search along this line was for the axial component of the velocity vector. The difference in the two consecutive axial positions where the axial velocity changed direction was taken as the length of the vortex. This procedure was conducted for different values of the flow obstruction, given by h/d .

Figure 6 presents the results obtained for the Taylor vortex length. The length of the vortex given in millimeters is presented in terms of the obstruction parameter h/d . The experimental results are represented in the figure by circles, while numerical results are represented by squares and triangle. The two numerical solutions differ on the boundary conditions imposed at the r - θ planes that limit the computation domain. As mentioned in the numerical solution section, three types of boundary conditions were utilized. In the figure, the squares represent boundary conditions of type (b), i.e., a symmetry plane at the mid-length of the annular space and no-slip boundary condition at the annular space end plane. The triangles represent boundary condition of type (c), where the full annular space constitutes the computation domain, and no-slip conditions are imposed at the two end planes.

It is interesting to verify in Fig. 6 that, although the results for critical Reynolds number presented in Fig. 5 were perfectly predicted by the numerical simulations, some discrepancy in relation to the experiments is observed in the prediction of the Taylor vortex length. A close observation of the results of Fig. 6 shows that, for some values of the obstruction, the agreement between simulation and experiments is very good, for type (b) boundary condition. This is the case for h/d equal to 0.375, 0.500, and 0.750. The same cannot be said for h/d equal to 0, 0.250, and 0.625. A considerable discrepancy is found for these values of h/d . A possible explanation for this behavior is related to the nature of the Taylor vortex flow in the annular space. The structure of the flow is formed by pairs of counter-rotating vortices. Thus, an even number of vortices is always expected to fill the length of the annular space. If a slight variation in the length of the vortices is obtained as a consequence of the imposition of a mathematically-based boundary condition, such as symmetry at the annular space mid-length, the solution will converge to the closest form where an even number of vortices can be accommodated. When this happens, a significant variation in vortex length is observed,

since a whole new vortex has to be accommodated in, or suppressed from the available annular space length. Since the vortex length is controlled by the dimension of the minimum flow passage given by the cylinder-to-plate distance, i.e. h/d , there are values of h/d in which the vortex length is such that a flow structure with even number of vortices close to the experimental condition is obtained. For other values of h/d , an entire vortex has to be accommodated or suppressed giving rise to the observed discrepancy on Taylor vortex length.

The influence of the boundary conditions on the Taylor vortices length was further investigated by running numerical simulations where the computational domain encompassed the whole length of the annular space. The boundary conditions imposed in this case were no slip at the solid vertical end caps that limit the annular space. These are labeled in Fig. 6 as boundary conditions of type (c). The computational time and memory requirements for a solution of this type are significantly larger than those required for a solution that employs boundary conditions of type (b) where just half of the physical domain is solved. For this reason, the tests with type (c) boundary conditions were run for the case where no flow obstruction was present, i.e., $h/d = 0$. For this case only, the natural circumferential symmetry of the problem allows the utilization of a two dimensional solution, thereby reducing the computational requirements.

The numerical result for Taylor vortex length employing boundary condition of type (c) is plotted as a triangle in Fig. 6 at the abscissa corresponding to $h/d = 0$. A perfect match with the experimental result is observed. The prediction of a Taylor vortex length of approximately 47.5 mm is exactly what was expected, since this is the dimension of the annular space in the experimental setup. The value obtained for the vortex length using boundary condition of type (b) is 46 mm. Although this difference might not seem significant, it should be mentioned that for type (c) boundary condition 52 vortices were obtained in the annular space, while 54 (27×2) vortices were obtained when type (b) boundary condition was employed. It should be mentioned that the numerical results obtained using type (a) boundary conditions were the same as those obtained using type (b) conditions. These results show that the symmetry condition at mid-length is the most relevant to the problem.

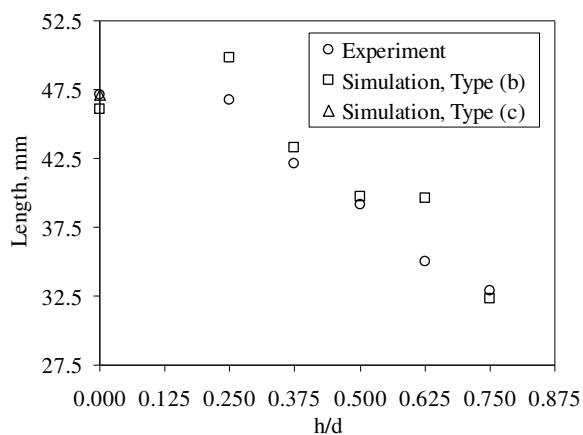


Figure 6. Vortex length versus annular obstruction for experiments and numerical simulation results.

A general observation of the results of Fig. 6 show that the length of the vortices decrease with h/d . Observations of vortex length, both numerical and experimental, at other circumferential positions demonstrated that the vortex length is constant all around the annular space. Experimental observations were made at meridional planes located at 0, 90, 180 and 270 degrees, as marked in Fig. 1. In order to conduct these measurements, the Plexiglas cylinder was manually rotated in relation to the horizontal laser light sheet, as described in the experiments section.

7. Taylor vortex characterization: axial velocity profile

Experimentally and numerically obtained axial velocity profiles will be presented for the free annular space and obstructed annular space configurations. The axial velocity profiles were obtained at an axial coordinate passing through the eye of the vortex located approximately at the mid-length of the annular space.

Figure 7 presents the axial velocity profiles for the annular space without obstruction. Results for two rotational Reynolds numbers are presented: 104 and 126. These values correspond, respectively, to 48 and 80% above the transition value, but below the values for the second transition to wavy-vortex regime for the radius ratio employed of 0.57. Two sets of representative experiments are presented in the figure. These are labeled group A and B experiments. These are experiments that were performed at the same nominal initial and boundary conditions but furnished different velocity profiles, as can be seen in Fig. 7(a) and 7(b). The experiments that compose these groups were carefully repeated using the same working fluid, at the same temperature. Further, the acceleration ramp imposed was the same for all experiments. The shaft was accelerated from rest up to the final value desired for the rotational Reynolds number imposing a low angular dimensionless acceleration equal to 10.2 ± 0.1 .

Since the camera that registered the particle images was kept at the same axial position in all experiments, the two types of velocity profiles measured are an indication of the existence of two stable solutions for the flow. An obvious observation in Fig. 7 is that the profiles for group A and group B experiments display opposite signs, indicating that a lateral shift in the vortices had occurred. Although it is not clear in the Figure, the group A and B profiles are not symmetric. Group A profiles display maximum axial velocities that are somewhat higher than those measured for group B experiments. This might be an indication of the presence of greater number of smaller, more intense vortices.

Figure 7 also displays numerical predictions of the axial velocity profiles. The boundary conditions employed in the calculations were of type (c), which means that the whole annular space was used as the computation domain with no-slip conditions at the end walls. The calculations were two-dimensional. The results show that the computer generated velocity profiles coincide with group B experiments for the two values of the Reynolds number investigated.

Figure 8 presents the axial velocity profiles for the obstructed annular space with $h/d = 0.5$, for Reynolds number of 108, which is about 22% above the transition value. The profiles are for an axial coordinate passing through the eye of the vortex. The dimensionless acceleration imposed on the shaft to reach the steady state condition was the same as in the free annular space, i.e., 10.2 ± 0.1 . Figure 8 corresponds to velocity profiles measured at meridional planes positioned at 0 and 180 degrees, while in Fig. 9 results for planes located at 90 and 270 degrees are presented.

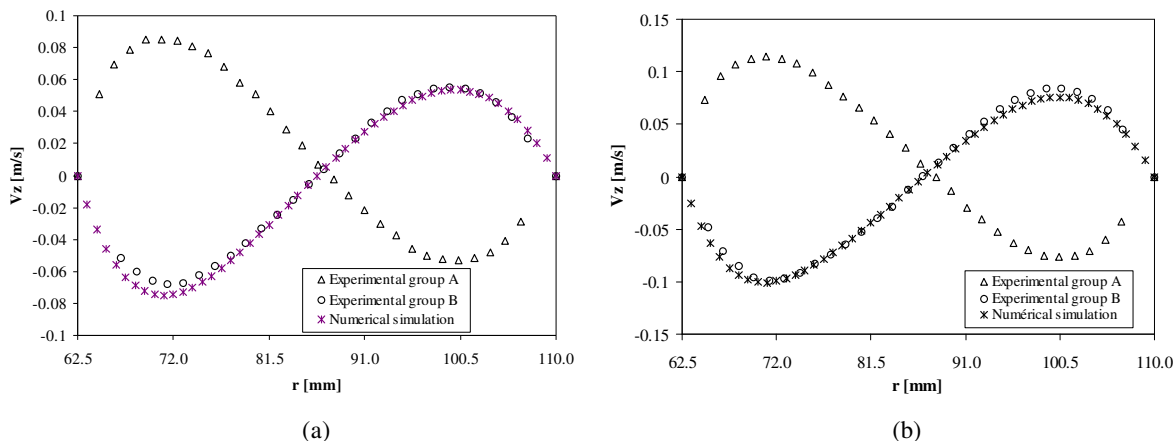


Figure 7. Axial velocity profiles for Taylor-Couette regime for free annular space. (a) $Re = 104$; (b) $Re = 126.1$.

It can be seen in the Figs. 8 and 9 that the same level of agreement between numerical and experimental results obtained for the free annular space case shown in Fig. 7 is achieved for the partially obstructed case. The boundary conditions employed in the calculations were of type (a), i.e., symmetry at mid-length and extended domain at the vertical end plane. The calculations were three-dimensional.

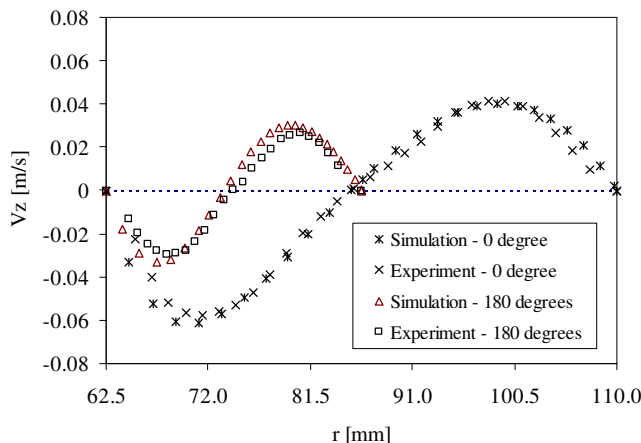


Figure 8. Velocity profile for Taylor-Couette regime in the meridional planes 0 and 180°. $Re = 109$, $h/d = 0.5$.

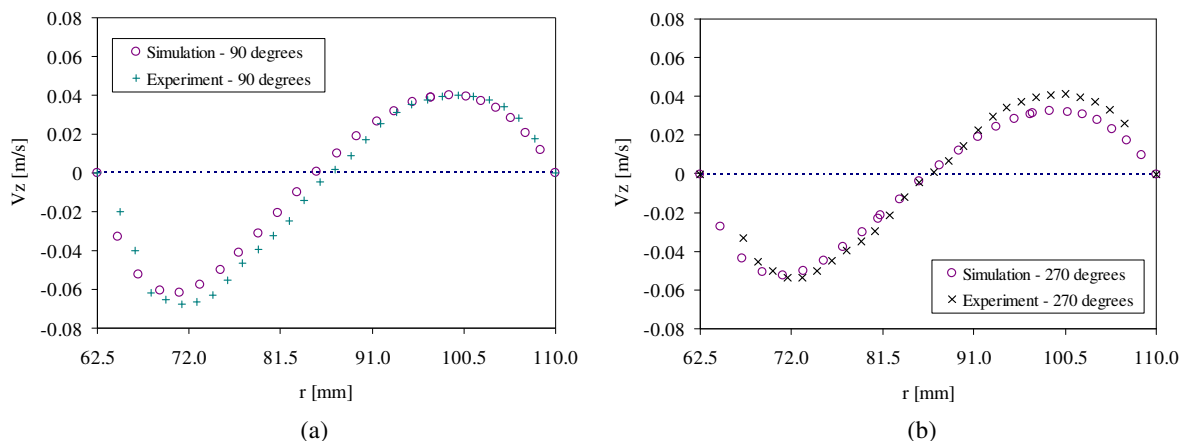


Figure 9. Velocity profile for Taylor-Couette regime in the meridional planes 90° and 270° . $Re: 109, h/d = 0.5$.

8. Taylor vortex characterization: Longitudinal velocity fields

The structure of the Taylor vortices present some additional characteristics that can be observed by a careful examination of the results obtained. Figure 10 presents the velocity field in a meridional plane r - z , for the annular space without obstruction, i.e., $h/d = 0$. In the figure the abscissa coincides with the surface of the inner rotating cylinder. The axial velocity profiles for a fixed axial position show that the magnitude of the velocity in the region close to the inner cylinder is greater than that for the region close to the outer cylinder. This observation is easier to be verified by examining Fig. 7 where the axial velocity profiles passing through the eye of the vortex are plotted. The explanation for this behavior of the axial velocity profiles is based on the requirement of mass conservation, since in the annular geometry the outer region of the gap offers a larger cross sectional area for the flow. This observation is also found in the work of Wereley and Lueptow [5].

The radial velocity component also displays a strong axial variation. Indeed, the magnitude of the radial velocity component is considerably larger in the region where radial flow is in the outward direction as compared to the region where the flow is directed toward the center of the annular section. To compensate this difference in magnitude and conserve mass, the flow area in the r - z plane is smaller for the outward directed flow. This observation can be verified in Fig. 10, where the boundary of the vortices indicate that they are more tightly spaced in the region of outward directed radial flow.

For the case of partially obstructed annular space, the structure of the flow becomes significantly more complex than the non-obstructed case. Figure 11 presents the numerical results obtained for a meridional plane located at the top of the annular space, i.e., at $\theta = 0$ degrees, for an obstruction characterized by $h/d = 0.75$. A general observation of the figure reveals a flow pattern similar to that presented in Fig. 11 for the non-obstructed case. However, the study of the flow in the transverse r - θ plane (not shown in the present paper) reveals that the circumferential velocity component reverses direction along the radial coordinate for a fixed axial coordinate. This is illustrated in Fig. 11 by the horizontal dashed line dividing the meridional plane in regions labeled as A and B. In region A the circumferential flow is directed into the plane of the paper, whereas in region B the flow is directed out of plane of the paper. This complex velocity field is generated by a recirculation zone induced in the r - θ plane by the obstruction imposed due to the presence of the plate.

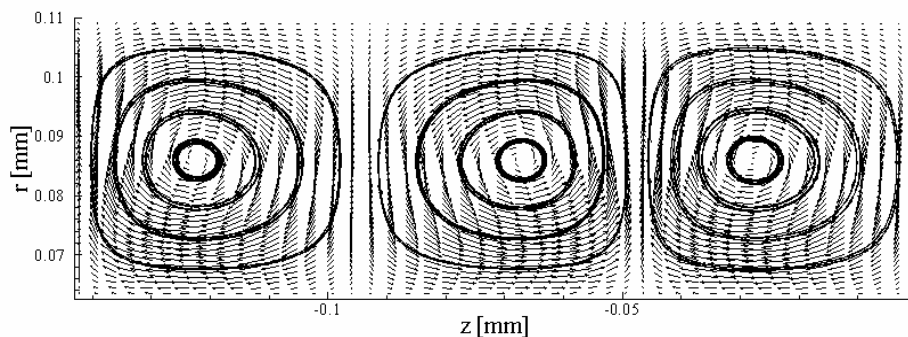


Figure 10. Velocity field in the r - z plane: Taylor vortex structure.

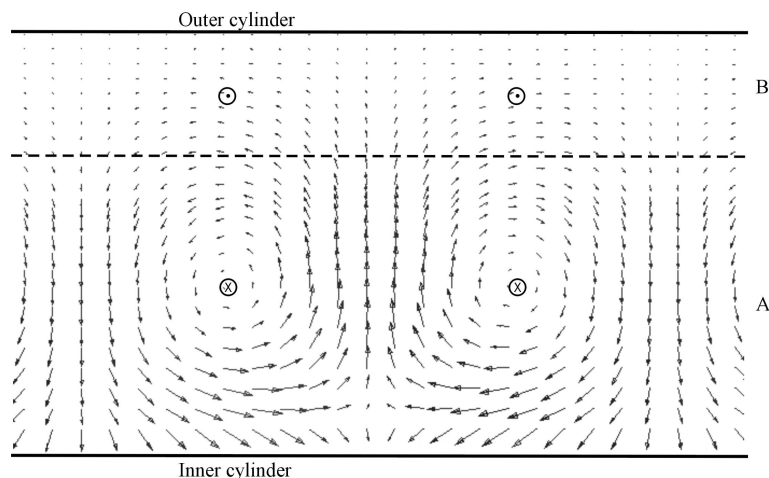


Figure 11. Numerically calculated velocity field in the r - z plane for $h/d = 0.75$

9. Concluding remarks

The present paper presented a combined numerical and experimental study of the flow characteristics of a horizontal Taylor-Couette flow with partial obstruction of the annular space. The obstruction was imposed by a horizontal plate positioned at the lower part of the annular gap. The presence of the plate destroys the circumferential symmetry of the problem and affects the transition from circular Couette to Taylor-vortex flow.

The three-dimensional velocity field within the annular space was determined by the numerical solution of the mass conservation and Navier-Stokes equations for incompressible, constant properties, Newtonian fluid at steady state conditions. Instantaneous and time-averaged velocity fields were determined experimentally by employing the particle image velocimetry technique, PIV.

The results obtained were in the form of critical values for the rotational Reynolds number that characterizes the transition from circular Couette flow to Taylor-vortex flow. Agreement between experimental and numerically predicted critical Reynolds numbers was excellent for all values of the cylinder-to-plate values investigated. The results have shown that the flow obstruction delays the transition to Taylor-vortex flow. A significant sensitivity of the critical Reynolds number to the acceleration imposed on the inner rotating cylinder was verified, which confirmed previous results available in the literature.

Excellent agreement was also found between computation and experiments for the axial velocity profiles. The experiments, however, revealed two possible different stable configurations for the velocity profiles for the annular space without obstruction. The existence of these solutions was attributed to a different number of vortices accommodated within the annular space length.

Although the agreement between computation and experiments was considered excellent for the critical Reynolds number and axial velocity profiles, the prediction of vortex length presented discrepancies between measured and predicted results, for some values of the cylinder-to-plate gap. Again, the discrepancies were attributed to the different number of vortex pairs accommodated within the annular gap. Different types of boundary conditions applied at the vertical end walls that seal the gap have shown to produce different number of counter-rotating pairs of vortices.

Numerically obtained velocity fields in the longitudinal, r - z , plane revealed the existence of a rather complex flow structure composed of Taylor vortices and zones of recirculating flow, when the flow passage between the cylinder and the horizontal plate is limited.

10. Acknowledgement

The authors acknowledge the support awarded to this research by the Rio de Janeiro State Research Foundation - FAPERJ, Brazilian Research Council - CNPq, Faculdade Centro Leste - UCL, and Petrobras S.A.

11. References

- Taylor, G.I., 1923, "Stability of a viscous liquid contained between two rotating cylinders", *Phil. Trans. Roy. Soc. A*, 223, 289-345.
- Cole, J.A., 1976, "Taylor-vortex Instability and Annulus-length Effects", *J. Fluid Mech.*, Vol.75, part 1, pp. 1-15.
- DiPrima, R.C., Eagles, P.M. and Ng, B.S., 1984, "The Effect of Radius Ratio on the Stability of Couette Flow and Taylor Vortex Flow", *Physics of Fluids*, Vol. 27, No. 10, pp. 2403-2411.

Andereck, C.D., Liu, S.S. and Swinney, H.L., 1986, "Flow Regimes in a Circular Couette System with Independently Rotating Cylinders", *J. Fluid Mech.*, Vol. 164, pp. 155-183.

Wereley S.T. and Lueptow, R.M., 1998, "Spatio-temporal Character of Non-wavy and Wavy Taylor-Couette Flow", *J. Fluid Mech.*, Vol. 364, pp. 59-80.

Lockett, T.J., Richardson, S.M. and Worraker, W.J., 1993, "The Importance of Rotation Effects for Efficient Cuttings Removal During Drilling", *SPE/IADC* 25768.

Philip, Z. Shama, M.M. and Chenevert, E., 1997, "The Role of Taylor Vortices in the Transport of Drill Cuttings", *SPE* 39504.

Sifferman, T.R. and Becker, T.E., 1992, "Hole Cleaning in Full-Scale Inclined Wellbores", *SPE Drilling Engineering*, pp. 115-120

Lim, T.T., Chew, Y. T. and Xiao, Q., 1998, "A New Flow Regime in a Taylor-Couette Flow", *Physics of Fluids*, Vol. 10, No. 12, pp. 3233-3235.

Park, K., Crawford, G.L. and Donnelly, R.J., 1981, "Determination of Transition in the Couette Flow in the Finite Geometries", *Physical Review Letters*, Vol. 47, No. 20, pp. 1448-1450.

DiPrima, R.C. and Stuart, J.T., 1972, "Non-local Effects in the Stability of Flow Between Eccentric Rotating Cylinders", *J. Fluid Mech.*, Vol. 54, Part 3, pp. 393-415.

Eagles, P.M., Stuart, J.T. and DiPrima, R.C., 1978, "The Effects of Eccentricity on Torque and Load in Taylor-vortex Flow", *J. Fluid Mech.*, Vol. 87, Part 2, pp. 209-231.

Coronado-Matutti, O. Souza Mendes, P.R. and Carvalho, M.S., 2004, "Instability of Inelastic Shear-Thinning Liquids in a Couette Flow Between Concentric Cylinders", *Journal of Fluid Engineering*, *In Press*.

Patankar, S.V., 1980, "Numerical heat transfer and fluid flow", Mc-Graw Hill.

Raffel, M., Willert, C. and Kompenhans, J., 1998, "Particle Image Velocimetry", Springer, 255p.

Gomes, B.A.A., Thompsom, R.L. and Azevedo, L.F.A., "Solid Body Rotation Flow for Particle Image Velocimetry Calibration", VIII Brazilian Thermal Science Congress, ENCIT, Porto Alegre, november 2000.